Available online at www.sciencedirect.com
SCIENCE DIRECT®
ACADEMIC PRESS
Icarus 164 (2003) 1–13
ICARUS
www.elsevier.com/locate/icarus

# Monte-Carlo simulation of Mercury's exosphere

Peter Wurz [a,*] and Helmut Lammer [b]

[a] *Physikalisches Institut, University of Bern, Sidlerstrasse 5, CH-3012 Bern, Switzerland*
[b] *Space Research Institute, Department for Extraterrestrial Physics, Austrian Academy of Sciences, Schmiedlstr. 6, A-8042 Graz, Austria*

Received 6 August 2002; revised 10 March 2003

**Abstract**

Because of its proximity to the Sun and its small size, Mercury has not been able to retain its atmosphere and only a thin exosphere surrounds the planet. The exospheric pressure at the planetary surface is approximately $10^{-10}$ mbar, set by the Mariner 10 occultation experiment. The existence of gaseous species H, He, and O has been established by Mariner 10. In addition Na, K, and Ca have been observed by ground based instrumentation. Other elements are expected to be found in Mercury's exosphere since the total pressure of the known species is almost two orders of magnitude less than the exospheric pressure.

It is intended to measure these exospheric particle densities in situ with an instrument on board of ESA's BepiColombo Mercury Planetary Orbiter (MPO) spacecraft. Since the expected exospheric densities are very small we developed a Monte-Carlo computer model to investigate if such a measurement is feasible along the MPO spacecraft orbit. We model energy and ejection angle distributions of the particles at the surface, with the emission process determining the actual distribution functions. Our model follows the trajectory of each particle by numerical integration until the particle hits Mercury's surface again or escapes from the calculation domain. Using a large set of these trajectories bulk parameters of the exospheric gas are derived, e.g., particle densities for various atomic and molecular species. Our study suggests that a mass spectrometric measurement is feasible and, at least at MPO's periherm, all species that are released from the surface will be observed.


*Keywords:* Mercury; Atmosphere; Composition; Exosphere

## 1. Introduction

Because of Mercury's proximity to the Sun and its small size, it has not been able to retain its atmosphere. However, the existence of gaseous species H, He and O has been observed by Mariner 10 (Broadfoot et al., 1976). In addition, the volatile components Na and K and later also Ca have been observed by ground based instrumentation (Potter and Morgan, 1985, 1986; Bida et al., 2000). Since the column content of the observed constituents is of the order of about $10^{12}$ cm$^{-2}$, which is less than the defined column content of an exosphere of about $10^{14}$ cm$^{-2}$, the gaseous envelope of Mercury represents an exosphere. It is expected that the six observed elements constitute only a small fraction of Mercury's exosphere because at the surface the total pressure from the sum of these known species is almost two orders of magnitudes less than the upper limit for the exospheric pressure of $10^{-10}$ mbar (Fjelbo et al., 1976; Hunten et al., 1988). Whereas H and He seem to have their origin in the solar wind, i.e., thermal release of implanted solar wind ions, heavier particles can be set free from the surface minerals by a variety of processes. These are thermal release, photon-stimulated desorption, particle sputtering and micrometeorite impact vaporization.

Before the Mariner 10 fly-by, it was generally thought that Mercury possesses a thin atmosphere similar in composition to Venus and Mars. It was argued that the terrestrial planets should have evolved along parallel lines and that a $CO_2$ atmosphere could be preserved by freezing out on the cool dark side (Fink et al., 1974). Therefore, Mariner 10 was designed to search for H, O, C, CO and $CO_2$, as well as the noble gases He, Ar and Ne. By scaling terrestrial noble gas production and diffusion rates and assuming a lunar-like solar wind surface interaction the before mentioned noble gases were thought to be the most abundant species (Hunten et al., 1988; Killen and Ip, 1999, and references therein).

The Mariner 10 spacecraft first encountered Mercury on 29 March 1974 and reencountered Mercury two more times,

* Corresponding author.
*E-mail address:* peter.wurz@soho.unibe.ch (P. Wurz).

0019-1035/03/$ – see front matter 
doi:10.1016/S0019-1035(03)00123-4

on 21 September 1974 and on 16 March 1975. From measurements with the UVS-instrument on Mariner 10 only H, He and O were observed in Mercury's exosphere (Broadfoot et al., 1976). A decade after the Mariner 10 fly-bys Potter and Morgan (1985) performed ground-based observations and discovered strong emission features at the Fraunhofer Na D lines in the spectrum of Mercury attributed to resonant scattering of sunlight from Na vapor in the planetary exosphere. They estimated a Na column density of $8.1 \times 10^{15}$ m$^{-2}$, which later was reduced to $1–3 \times 10^{15}$ m$^{-2}$ (Killen et al., 1993). Later the existence of suprathermal Na in Mercury's exosphere has been reported by Potter and Morgan (1997a), e.g., "an extended Na exosphere," which reaches more than a planetary radius above the surface. Using a barometric model at a temperature of 6500 K gives a surface density $n_0 = 500$ atoms cm$^{-3}$ (Potter and Morgan, 1997a), which corresponds to a column density of $1.7 \times 10^{13}$ m$^{-2}$ for the reported temperature. This is about a factor of 100 less than the main Na exospheric component. A detailed study of the Na tail directed in the anti-sunward direction, which results from the anti-sunward acceleration of these suprathermal Na atoms by solar photons, has been recently published (Potter et al., 2002). The existence of such a Na tail was predicted by Ip (1986) based on a Monte-Carlo model.

Careful observations of the Na D line profiles suggest that Na in the exosphere is hotter than the surface, i.e., Na is not accommodated with the surface temperature (e.g., Potter and Morgan, 1985; Smyth, 1984; Hunten et al., 1988). A detailed study of Na line profiles by Killen et al. (1999) revealed that the Na gas is indeed hotter than the surface by 600–700 K everywhere. These authors also gave an upper limit for energetic, e.g., suprathermal, Na atoms in the exosphere of 1%, which is in good agreement with the extended exosphere reported earlier by Potter and Morgan (1997a).

Potter and Morgan discovered also small concentrations of K in Mercury's exosphere, about a factor of 200 less than Na (Potter and Morgan, 1986, 1997b). Ca was discovered as the sixth element in Mercury's exosphere, and its existence in the exosphere was attributed to sputtering because of its proximity to Mercury's poles, the high temperature, and the temporal variability (Bida et al., 2000).

It was suggested that solar wind ion sputtering may account for part of the Na and K in the exosphere because of the localization at high northern and southern latitudes at the day side and the rapid temporal changes of the population of the order of a day and less (Potter and Morgan, 1997a; Potter et al., 1999). In addition, diurnal variations of Na and K column abundances have been observed (Sprague et al., 1997), with morning and midday Na column abundances a factor of three larger than in the afternoon. Based on a four-year data set of observations of Na at Mercury, Sprague et al. (1997, 1998) reported correlations of increased Na column abundances with large surface features, like the Caloris basin or some radar bright spots.

With the magnetometer on-board Mariner 10 it was found that Mercury possesses a small magnetosphere due to its intrinsic magnetic field (e.g., Ness et al., 1974, 1976; Ogilvie et al., 1974). It is assumed that a direct interaction of the solar wind with the planet surface is very unusual, because the magnetosphere is holding off the solar wind most of the time (see reviews by Russell et al., 1988; Wurz and Blomberg, 2001). Based on studies using different magnetospheric models it has been argued that Mercury's magnetosphere could be open to the solar wind over significant areas when the interplanetary magnetic field turns southward (Luhmann et al., 1998; Sarantos et al., 2001; Killen et al., 2001; Massetti et al., 2002). Solar wind particles can therefore reach the surface where they act as sputtering agents for surface particles. Lammer and Bauer (1997) showed that particle sputtering could be a source of hot Na atoms with ejection speeds larger than 2 km s$^{-1}$. Micrometeorite impact vaporization could also be responsible for hot components in Mercury's exosphere (e.g., Cheng et al., 1987; Morgan et al., 1988, 1989; Sprague, 1990; Cintala, 1992; Killen et al., 2001).

A more astounding and unexpected discovery was made in radar measurements of Mercury where radar bright regions near the poles were found (Harmon and Slade, 1992). These regions have been used to argue for the presence of condensed volatile species in a manner analogous to that suggested for permanently shadowed regions on the Moon. These areas were originally attributed to $H_2O$ ice (Harmon and Slade, 1992). Contrary to that it has been suggested that cold silicate minerals would also produce similar results (Starukhina et al., 2000). The chemical nature of such volatile deposits on Mercury was proposed to be either water-ice (Harmon and Slade, 1992; Harmon et al., 2001), elemental sulfur (Sprague et al., 1995), or even Na (Harmon and Slade, 1992). Direct measurements by instrumentation on ESA's planned Mercury Surface Element (MSE), and remote observations of Mercury's surface using X-ray and optical spectroscopy as well as in situ measurements of the exospheric composition from an orbiting spacecraft, like the Mercury Planetary Orbiter (MPO) of the BepiColombo mission, could resolve the controversy and help to explain the cycling of volatile elements between Mercury's interior, surface mineralogy and exosphere, and the contribution of meteoritic and cometary material to Mercury's near-surface volatile budget.

In this paper we present a new Monte-Carlo simulation of Mercury's exosphere. We calculate the exospheric densities by using a Monte-Carlo technique, which has the advantage that different particle release processes from Mercury's surface can be modeled. Depending on the species, we simulate thermal release, photon-sputtering, particle sputtering and micrometeorite impact vaporization to release particles into the exosphere. From the obtained density profiles we can evaluate whether an instrument measuring the exospheric gas composition in situ by mass spectrometric means, like the measurement analyzer for atoms and ions (MAIA) in-

strument proposed for the MPO spacecraft (Mildner et al., 2001), will have sufficient sensitivity to measure the elemental, chemical and isotopic composition of Mercury's exosphere along the MPO orbit and assess how well such measurement could be done.

## 2. Particle source processes

Particles are directly released from Mercury's surface into the exosphere by a variety of processes. The possibilities are thermal release, particle sputtering, photon-sputtering, and micrometeorite impact. Depending on the species, local time (Hermean day), orbital position (Hermean year), and solar wind conditions, different processes will be important for the particle release. These processes have been discussed widely over the years (e.g., Killen and Ip, 1999; Lammer and Kolb, 2001, and references therein). Na is the best studied element in terms of the different release processes (e.g., Killen et al., 2001).

Our Monte-Carlo model assumes angular and velocity distributions at the surface in three dimensions as prescribed by the release process and follows the individual trajectories of the particles through the exosphere until the particles hit the surface or escape from the planet. A particle falling back onto the surface is considered lost since the high porosity of the surface, and the associated large surface corrugation, makes it very unlikely that these particles are directly reflected back into the exosphere. Rather, the particles will be thermalized and possibly efficiently trapped in the soil. For example, the porosity of the surface of the moon is 0.5 (Heiken et al., 1991) and even higher porosities for the Hermean surface have been considered (Killen et al., 2001). In the model, no assumptions are made for the exosphere itself, for example barometric scaling or nonbarometric scaling; everything follows from the trajectory calculations. In our calculations we consider all species listed in the review paper by Killen and Ip (1999) and which we reproduced in Table 1 together with the model parameters we used. The way we implement the different processes is detailed below.

Thermal release will be responsible for the diffusion to the surface and the release of volatiles into the exosphere. In our model, species released thermally are H, He, Ar, Ne, $H_2$, $O_2$, $N_2$, $H_2O$, OH, and $CO_2$. Probably H and He originate mostly from the solar wind in a similar way as on the Moon (e.g., Hinton and Taeusch, 1964; Johnson, 1971; Hodges, 1973, 1980). The other species listed above originate from Mercury, either diffusing through the crust or evaporating from condensed volatiles. The solar wind ions can penetrate the Hermean magnetosphere on open magnetic field lines, the cusp region, and reach the planetary surface where they become implanted into the soil at locations associated with these areas of open magnetic field lines. Implanted H and He will migrate to the surface by diffusion driven by the surface temperature and thermally desorb into the exosphere. In the case that solar wind H and He particles are reflected from the

Table 1
Input parameters for the Monte-Carlo calculations for the considered species

| Compound | Surface density ($m^{-3}$) | Column density ($m^{-2}$) | Temperature (K) | Surface binding energy, $E_b$ (eV) |
|---|---|---|---|---|
| H[a] | $2.3 \times 10^7$, $2.3 \times 10^8$ | – | 420, 100 | – |
| He | $6.0 \times 10^9$ | – | 575 | – |
| O | $4.4 \times 10^{10}$ | – | – | 3.4 |
| Na[b] | – | $2.0 \times 10^{15}$ | 1100 | – |
| Na[c] | – | $1.7 \times 10^{13}$ | – | 1.2 |
| K | – | $1.0 \times 10^{13}$ | 900 | – |
| K | – | $9.0 \times 10^{10}$ | – | 2.4 |
| Ar | – | $6.6 \times 10^{12}$ | 540 | – |
| Ne[d] | $6.0 \times 10^9$, $7.0 \times 10^{11}$ | – | 540, 110 | – |
| $H_2$ | $2.6 \times 10^{13}$ | – | 540 | – |
| $O_2$ | $2.5 \times 10^{13}$ | – | 540 | – |
| $N_2$ | $2.3 \times 10^{13}$ | – | 540 | – |
| $CO_2$ | $1.6 \times 10^{13}$ | – | 540 | – |
| $H_2O$ | $1.5 \times 10^{13}$ | – | 540 | – |
| OH | $1.5 \times 10^{11}$ | – | 540 | – |
| Mg | – | $3.9 \times 10^{14}$ | – | 2.4 |
| Ca | – | $1.1 \times 10^{12}$ | – | 2.1 |
| Fe | – | $7.5 \times 10^{12}$ | – | 2.4 |
| Si | – | $1.2 \times 10^{14}$ | – | 2.4 |
| S | – | $2.0 \times 10^{14}$ | – | 2.4 |
| Al | – | $3.0 \times 10^{13}$ | – | 2.4 |

Compositional data are taken from Killen and Ip (1999) and from Bida et al. (2000); for temperatures and surface binding energies see text. Some of the surface or column densities are upper limits.

[a] The measured Mariner 10 data was best reproduced by a hot and a cold component (Hunten et al., 1988; Killen and Ip, 1999, and references therein).

[b] Killen and Ip (1999) give a range of $1.7–3.8 \times 10^{10}$ $m^{-3}$.

[c] Suprathermal (sputtered) Na component of $T_0 \approx 6500$ K (Potter and Morgan, 1997a).

[d] Day- and night-side surface densities (Killen and Ip, 1999).

surface (as neutrals), we assume in our model complete accommodation with the surface temperature, e.g., resampling a Maxwellian-like distribution. Since it is very likely that the surface material is a fine grained soil with particles sizes of 100 μm and less (Langevin, 1997; Cooper et al., 2001), the probability of localized multiple collisions is high and hence accommodation is likely.

For the supply of less volatile and refractory species into Mercury's exosphere photon-stimulated desorption, meteoritic impact vaporization, and sputtering are generally assumed. Thermal release, photon-stimulated desorption and meteoritic impact vaporization are active exospheric source processes happening all the time, with the former two having a pronounced day-night modulation. On the other hand, the average meteoritic influx on Mercury, is presumed to be isotropic over the whole planet (e.g., Killen et al., 1999, 2001). Increased sputtering by solar wind ions results when the magnetosphere opens its field lines in response to a southward interplanetary magnetic field or at unusually large solar wind dynamic pressure. Solar wind ions will enter at the cusp regions (Luhmann et al., 1998; Sarantos et al., 2001; Killen et al., 2001; Massetti et al., 2002) and lead to a rapid increase in contents of surface sputtered particles in the exosphere. Sputtering by magnetospheric ions from the tail region may occasionally contribute material to the exosphere at the night-side from selected locations. During quiet days, that is during times of no precipitation of solar wind or magnetospheric ions onto the planet's surface, thermal release, photon-stimulated desorption and meteoritic impact vaporization will be the only processes populating the exosphere. By performing measurements on the night-side one almost exclusively studies micrometeoritic impact vaporization.

### 2.1. Photon-stimulated desorption

Photon-stimulated desorption (PSD), which sometimes is referred to as photon sputtering, of sodium was the first process proposed as a major source of Na in the Hermean exosphere (McGrath et al., 1986). That the Na distribution peaks at the sub-solar point at times was considered good evidence for PSD (Killen et al., 1990). We will also use PSD to model the main Na exosphere. Yakshinskiy and Madey (1999) found in laboratory studies that Na atoms can be released via PSD from surfaces that simulate lunar silicates. They found that bombardment of such surfaces at temperatures of about 250 K by ultraviolet photons with wavelengths $\lambda < 300$ nm causes very efficient desorption of Na atoms. It was found that the photon-stimulated desorption is induced by electronic excitations rather than by thermal processes or momentum transfer. However, the surface temperature will be responsible for diffusion of material to the surface.

Killen et al. (1999) found that sodium in the exosphere appears to be hotter than the surface by about 600–700 K everywhere. The energies associated with these Na gas temperatures are consistent with laboratory measurements of velocity distributions for PSD. Yakshinskiy and Madey (2001a, 2001b) found for PSD of Na and K velocity distributions peaking at 1000 and 650 $\mathrm{m\,s^{-1}}$ for desorption from $SiO_2$, respectively, and peaking at 800 and 500 $\mathrm{m\,s^{-1}}$ for desorption from ice (at ≈100 K). A good mathematical description of these velocity distributions has been given by Johnson et al. (2002), which we use in our model

$$f_{\mathrm{PSD}}(E) = \beta(1+\beta)\frac{EU^{\beta}}{(E+U)^{2+\beta}} \tag{1}$$

with $E$ the particle energy, $U$ the characteristic energy for PSD for a particular species, and $\beta$ the shape parameter of the distribution ($\beta_{\mathrm{Na}} = 0.7$ and $\beta_{\mathrm{K}} = 0.25$ (Johnson et al., 2002)). The peak in the Na velocity distribution reported by Yakshinskiy and Madey (2001a, 2001b) agrees well with the Na temperatures deduced from line widths of Na in Mercury's exosphere (Killen et al., 1999). Therefore, we use in our model for PSD of Na and K characteristic energies $U$ derived from a temperature which is 600 and 400 K above the Hermean surface temperature.

Only volatile species, mostly Na and K, will be released into the exosphere via PSD. Water may also be released by PSD and possibly sulfur if exposed to sunlight. These species may be present at the poles (see discussion above) and are most likely buried under a layer of regolith but may be brought to the surface by meteoritic impact, for example. In summary, PSD is highly nonstoichiometric in reproducing the composition of the surface in the exosphere.

We can calculate the flux of photon-stimulated desorption of Na atoms $\phi_{\mathrm{Na}}^{\mathrm{PSD}}$ from

$$\begin{aligned}\phi_{\mathrm{Na}}^{\mathrm{PSD}} &= f_{\mathrm{Na}} N_{\mathrm{S}} \int \phi_{\mathrm{ph}}(\lambda)\, Q_{\mathrm{Na}}(\lambda)\, \mathrm{d}\lambda \\ &\approx \frac{1}{4}\phi_{\mathrm{ph}} Q_{\mathrm{Na}} f_{\mathrm{Na}} N_{\mathrm{S}},\end{aligned} \tag{2}$$

where the factor 1/4 gives the surface-averaged value. $\phi_{\mathrm{ph}}$ is the solar UV photon flux at Mercury, $Q_{\mathrm{Na}}$ is the PSD cross-section, $N_{\mathrm{S}}$ is the regolith surface density, and $f_{\mathrm{Na}}$ is the sodium fraction in the regolith. The experimentally determined PSD cross-section for Na is $Q_{\mathrm{Na}} = 1\text{–}3 \times 10^{-20}$ $\mathrm{cm^2}$ in the wavelength range of 400–250 nm (Yakshinskiy and Madey, 1999). The regolith surface density is assumed to be $N_{\mathrm{S}} = 7.5 \times 10^{14}$ $\mathrm{cm^{-2}}$ with a sodium fraction in the regolith of $f_{\mathrm{Na}} = 0.0053$ (Killen et al., 2001). The solar UV photon flux at 0.38 AU integrated over the wavelength range from 0.1–318.0 nm is $\phi_{\mathrm{ph}} = 3.31 \times 10^{15}$ $\mathrm{cm^{-2}\,s^{-1}} \times (1/0.38)^2 = 2.29 \times 10^{16}$ $\mathrm{cm^{-2}\,s^{-1}}$ (Jursa, 1985). Using these values Eq. (2) evaluates to a PSD flux of Na atoms of $\phi_{\mathrm{Na}}^{\mathrm{PSD}} \approx 4.1 \times 10^{12}$ $\mathrm{m^{-2}\,s^{-1}}$. With an average release velocity of $v = 1000$ $\mathrm{m\,s^{-1}}$ (Yakshinskiy and Madey, 2001a, 2001b) we get an exospheric density at the surface of $n_0 = 4.1 \times 10^9$ $\mathrm{m^{-3}}$. We can compare this exospheric density at the surface with the measured column density of $n_{\mathrm{C}} = 2 \times 10^{15}$ $\mathrm{m^{-2}}$ (Killen and Ip, 1999). Assuming $U = 0.098$ eV in Eq. (1) (corresponding to a temperature $T_0 = 1100$ K, sub-solar point) results in an exospheric density at the surface of $6.8 \times 10^9$ $\mathrm{m^{-3}}$ using our Monte-Carlo code. The two exospheric surface

densities compare well, considering that there is an increase in PSD cross-section for wavelengths short of 300 nm, which we did not include, and the Mercury regolith surface density may be on the small side.

Since we are mostly interested in the exospheric densities near the planet, at the orbit of the BepiColombo/MPO spacecraft of 400 × 1500 km, and are not interested in the exospheric tail extending more than 10 planetary radii in the anti-sunward direction (Potter et al., 2002), we did not consider the change of trajectories by photon pressure and the loss of particles due to photo-ionization. These two processes mainly affect Na and K, and much less all the other species. For Na the photo-ionization lifetime is 5.5–$16.9 \times 10^4$ s at Mercury's pericenter (see Potter et al., 2002, and references therein). The travel times to an altitude of 1500 km, which only few particles reach, are of the order of $10^3$ s. For K the photo-ionization lifetime is $\approx 10^5$ s at Mercury's pericenter and for the other species it is even larger by an order of magnitude (Kumar, 1976; Killen and Ip, 1999). Using an extensive set of observations, Sprague et al. (1997) found no correlation of the column densities with radiation pressure and concluded that "radiation acceleration is not the major factor influencing the distribution of Na about the planet's sunlit hemisphere."

### *2.2. Solar wind supply*

The solar wind ions can impinge on the planet's surface by direct penetration through the cusp regions under favorable orientations of the interplanetary magnetic field (Luhmann et al., 1998; Sarantos et al., 2001; Killen et al., 2001; Massetti et al., 2002), and act as sputtering agents (e.g., Hodges, 1973, 1980; Killen and Ip, 1999). The solar wind ion flux at the surface is expected to vary as the magnetosphere responds to the solar wind density and velocity and the orientation of the interplanetary magnetic field (e.g., Luhmann et al., 1998; Kabin et al., 2000; Sarantos et al., 2001). Long time observations of Na column contents showed that Mercury's exosphere is temporally and spatially highly variable (Potter and Morgan, 1997a; Potter et al., 1999). The authors found during a week-long observation from 13 to 20 November 1997, that the total Na content in Mercury's exosphere increased by a factor of three and that the spatial distribution varied daily. Potter et al. (1999) and later Killen et al. (2001) concluded that the rapid variations in the Na content during that time period are coupled to solar wind-magnetospheric interactions. Magnetospheric ions hitting the planet's surface at the auroral zones will also cause sputtering. The suprathermal Na atoms, i.e., extended Na exosphere (Potter and Morgan, 1997a) and the Ca exosphere (Bida et al., 2000) are considered to be results of particle sputtering. In general, probably all refractory elements will be introduced into the exosphere via particle sputtering during times of ion precipitation.

One can estimate the total flux of precipitating solar wind particles onto Mercury's surface as:

$$\Phi_{\rm sw} = C \rho_{\rm sw} v_{\rm sw} A_{\rm s}, \tag{3}$$

with solar wind density $\rho_{\rm sw}$, the solar wind velocity $v_{\rm sw}$ and the surface area $A_{\rm s}$ associated with open magnetic field lines. The factor $C$ in Eq. (3) reflects the assumed difference of the surface area with open field lines and the corresponding area in the undisturbed solar wind. Goldstein et al. (1981) estimated a maximum flux of solar alpha particles precipitating along open field lines of about $9 \times 10^{23}$ s$^{-1}$ by scaling an Earth magnetospheric model. Recent model calculations show that by using $C = 4$ (Killen et al., 2001) the fluxes given by Eq. (3) represent peak fluxes and the average solar wind flux propagating onto Mercury's surface along open field lines is markedly lower (Massetti et al., 2002).

The local solar wind flux at locations of open field lines, $\phi_{\rm sw} = \Phi_{\rm sw}/A_{\rm s}$, is estimated from Eq. (3) as $\phi_{\rm sw} \approx 10\ {\rm cm}^{-3}/(0.38)^2 \times 400\ {\rm km\,s}^{-1} = 2.8 \times 10^{13}\ {\rm m}^{-2}\,{\rm s}^{-1}$ with $C = 1$. Using a weighted sputter yield of the solar wind at 1 keV/nuc of $Y_{\rm tot} = 0.15$ per solar wind ion (for the mix of H, He, O, ... Fe) we get the sputtered flux as $\phi_{\rm sput} \approx 4.2 \times 10^{12}\ {\rm m}^{-2}\,{\rm s}^{-1}$. With a typical energy of the sputtered Na particles of 0.6 eV, corresponding to the temperature of $T_0 = 6500$ K of the suprathermal Na atoms, i.e., the extended Na exosphere (Potter and Morgan, 1997a), we get an exospheric surface density of Na of $n_0 = 1.9 \times 10^9\ {\rm m}^{-3}$ from this simple estimate using the regolith density from above. Taking a column density of $n_C = 4 \times 10^{15}\ {\rm m}^{-2}$ attributed to sputtering in the November 1997 observations (Potter et al., 1999) we get an exospheric surface density of $n_0 = 2.1 \times 10^9\ {\rm m}^{-3}$ from our Monte-Carlo code using a Na surface binding energy $E_{\rm b} = 1.2$ eV (see below). Given the accuracy with which the individual parameters can be estimated we feel that the agreement is reasonable.

### *2.3. Particle sputtering*

Sputtering from a solid planetary surface is calculated in exact analogy with sputtering from an atmosphere (Sieveka and Johnson, 1984; Johnson, 1990; Lammer and Bauer, 1997). It produces particles that can directly escape or, if their velocity is insufficient, the particles move along ballistic trajectories. The energy distribution for particles sputtered from a solid, $f(E_{\rm e})$, with the energy $E_{\rm e}$ of the sputtered particle, has been given as (Sigmund, 1969):

$$f(E_{\rm e}) \propto \frac{E_{\rm e}}{(E_{\rm e} + E_{\rm b})^3} \left\{ 1 - \left[ \frac{(E_{\rm e} + E_{\rm b})}{E_{\rm i}} \right]^{1/2} \right\}, \tag{4}$$

where $E_{\rm b}$ is the surface binding energy of the sputtered particle and $E_{\rm i}$ the energy of the incident, the projectile, particle. Note that the maximum of the energy distribution is at $E_{\rm max} = E_{\rm b}/2$.

Particle sputtering will release all species from the surface into space reproducing more or less the local surface

composition on an atomic level. Preferential sputtering of the different elements of a compound will lead to a surface enrichment of those elements with low sputtering yields. However, the steady-state composition of the flux of sputtered atoms will reflect the average bulk composition. Thus, particle sputtering, when operative, will give us information also about the refractory elements of the surface, for example the Ca exosphere that was observed over the poles (Bida et al., 2000).

Sputtering by solar wind ions will only occur for restricted time intervals when the interplanetary magnetic field is oriented favorably or the solar wind dynamic pressure is very high. Even under favorable conditions only a few percent of Mercury's surface are associated with open magnetic field lines (Massetti et al., 2002). However, the solar wind also has a neutral component, at Earth orbit its flux is $10^{-4}$–$10^{-3}$ of the ion flux (Collier et al., 2001). The neutral solar wind (NSW) is not deflected by the Hermean magnetosphere and thus permanently causes sputtering on the entire dayside of the planet. At Mercury's orbit the NSW fraction may be lower than at Earth orbit, perhaps less than $10^{-4}$, but the larger area and the continuous presence of the NSW may yield sputter fluxes comparable to the sputter fluxes resulting from solar wind ions.

### 2.4. Micrometeorite impact vaporization

Micrometeorite impacts may contribute to the production of exospheric densities, including low-volatile and refractory species. Especially during quiet times, i.e., without energetic ions from the magnetosphere or the solar wind hitting the surface, it may be the only release process acting over the whole planetary surface. The impact of micrometeorites will evaporate a certain volume from Mercury's surface to the exospheric gas at the impact site. About one to two orders of magnitude more material than its own is released because of the high impact speed for meteorites at Mercury (Cintala, 1992). Unfortunately, the infall of meteorites will have contaminated the Hermean surface at a level of 1% to 10% over the billion of years of bombardment. The meteorites will consist of mainly refractory material since the meteorite population in the inner solar system is not as rich in $H_2O$ and other volatiles as in the outer solar system, which is more cometary-like being supplied from cometary matter having their origin in the Kuiper Belt (Divine, 1993).

The ratio of the maximum ejecta velocity to the primary impact velocity decreases with increasing impact speed. The measured temperature in the micrometeorite produced vapor cloud is in the range of 2500–5000 K (Eichhorn, 1978a). Such temperatures are up to a factor ten higher than Mercury's dayside surface temperature. The corresponding characteristic energies are still lower than for particles that result from surface sputtering. We use for the simulation of trajectories for particles that have their origin in micrometeorite vaporization a Maxwellian-like energy distribution with an average gas temperature of about 4000 K.

For the determination of the micrometeoroid energy density distribution we need the mean temperature of the ejected or vaporized meteoroid cloud. Eichhorn (1978a, 1978b) studied the velocities of impact ejecta parameters during hypervelocity primary impacts. He found that the velocity of the ejecta increases with increasing impact velocity and decreasing ejection angle, with the ejection angle measured with respect to the plane of the target surface.

As an example, the number of Na and K atoms added to Mercury's exosphere via impact-driven supply each second can be estimated from the mass of the infalling material per second and the meteorite impact velocity. Further, the elemental abundance of Na and K in Mercury's surface regolith and in the micrometeorite population regulate the number of Na and K atoms that are added to the exospheric particle population (Morgan et al., 1988). Cintala (1992) estimated the total vaporization for Mercury to range from $8.18 \times 10^{-16}$ to $2.75 \times 10^{-15}$ g cm$^{-2}$ s$^{-1}$ for aphelion and perihelion, respectively. Later, using a higher mass influx and considering surface porosity, Killen et al. (2001) estimated the total impact vaporization rates on diabase regolith and found vaporization rates between $9.0 \times 10^{-16}$ to $1.6 \times 10^{-14}$ g cm$^{-2}$ s$^{-1}$. From the total vaporization rates Na vaporization rates can be estimated that correspond to fluxes of released Na atoms, which range from $1.3 \times 10^{9}$ to $2.2 \times 10^{10}$ m$^{-2}$ s$^{-1}$. With the most probable speed of Na at 4000 K we get exospheric surface gas densities of Na ranging from $n_0 = 7.2 \times 10^{5}$ m$^{-3}$ to $n_0 = 1.3 \times 10^{7}$ m$^{-3}$. These densities have to be compared with the exospheric surface density for quiet times of $2.1 \times 10^{10}$ m$^{-3}$ derived from observations (see above). The comparison based on exospheric surface density is unfavorably distorted by the different velocities of the released atoms for the various processes and comparing the column densities is more objective. Anyway, aside from the uncertainties of the estimate, the contribution to the exosphere by impact-vaporization appears to be one or two orders of magnitude smaller than by other processes, when these processes operate. Impact vaporization may only be relevant at the night-side of the planet. However, since it is a vaporization process setting free a whole volume of the surface it holds the hope that the resulting exosphere reflects the surface composition including the chemical compounds even better than sputtering.

### 2.5. Generation of thermal particle velocity distributions

Since several release processes result in thermal distributions of the exospheric particles, either at the local surface temperature or at some elevated temperature, we create such a distribution by using Gaussian deviates. A set of three Gaussian deviates is needed to determine the components of a velocity vector for the thermal particle release at the surface. The Gaussian deviates, denoted $G_i$, are calculated by using the relation given in (Zelen and Severo, 1965; Hodges, 1973):

$$G_i = \left[-2\ln(p_i)\right]^{1/2} \cos(2\pi q_i), \tag{5}$$

where $p_i$ and $q_i$ are uniform deviates between 0 and 1. The variance of each $G_i$ is 1 (for $i = 1, 2, 3$). The initial velocity vector, $\mathbf{v}_0 = (v_1, v_2, v_3)$, at the start of the particle trajectory is

$$\mathbf{v}_0 = \left(\frac{m}{k_B T_0}\right)^{1/2} \mathbf{G} + \mathbf{r} \times \mathbf{\Omega}, \tag{6}$$

with particle mass $m$, the Boltzmann constant $k_B$, $T_0$ the main temperature of the released particle, $\mathbf{r}$ the release location on the surface, and $\mathbf{\Omega}$ the rotation of the planet. The particle velocity $v_0$ at the point of origin on Mercury's surface is $\sqrt{\mathbf{v}_0^2}$. The main temperature $T_0$ is taken either as local surface temperature at the particle release site or as characteristic temperature of the release process as discussed above. According to infrared measurements on Mariner 10 (Chase et al., 1976) the day-side temperature follows a "1/4" law with $T_{\max}$ the temperature at the sub-solar point and $T_{\min}$ the night-side temperature. Thus we can write the local surface temperature as

$$T_0(\phi, \theta) = \begin{cases} T_{\min} + (T_{\max} - T_{\min})(\cos\phi \cos\theta)^{1/4}, \\ \quad 0 < |\theta| < \pi/2, \\ T_{\min}, \quad \pi/2 < |\theta| < \pi, \end{cases} \tag{7}$$

with the longitude $\theta$ being measured from the planet-sun axis and the latitude $\phi$ measured from the planetary equator.

### 2.6. Generation of sputtered particle velocity distributions

For the generation of the energy distributions of particles released via sputtering or via PSD we employ the transformation method. Instead of Eq. (4) we use for our model simulations the simpler form

$$f_E(E_e) = \begin{cases} 2E_b \frac{E_e}{(E_e + E_b)^3}, & \text{if } E_e < E_i, \\ 0, & \text{otherwise.} \end{cases} \tag{8}$$

The difference between Eqs. (4) and (8) is only noticeable at energies close to $E_i$, where the probability is very low anyway. Note that Eq. (8) is normalized. By multiplying $f_E(E_e)$ with the total sputter yield $Y_{\text{tot}}$ for primary particles of energy $E_i$ we obtain energy resolved absolute sputter yields. Similarly, we obtain energy resolved PSD yields by multiplying $f_{\text{PSD}}(E)$ with Eq. (2). Starting from the surface composition is not considered further in this study, aside from the estimates given above, because there are no data available for the surface composition, since no spacecraft ever landed on Mercury. Moreover, remote sensing did not yield any useful data on surface composition because of observational difficulties. In our follow-up study we investigated the release of particles by sputtering and PSD all the way from the surface into the exosphere (Lammer et al., 2002).

Equations (1) and (8) can be integrated easily and the integral can be inverted. Using a uniform distribution in the interval [0, 1] as input for the inverted integral we get the desired distribution of random values with probability matching Eqs. (1) and (8). The same approach is taken for the elevation angle distribution for sputtering that is $f_\alpha \propto \cos(\alpha)^n$ with $n$ being 2 (Hofer, 1991). For the azimuth angle we used a uniform distribution over $2\pi$. Having the energy, the azimuth and elevation angle we can calculate all three components of the initial particle velocity $\mathbf{v}$.

## 3. Particle energy and ejection angle distributions

The particles released from Mercury's surface are moving mainly on ballistic trajectories. Trajectory modifications due to radiation pressure are not considered in the present model. From the many elements found and expected in Mercury's exosphere only Na and K are strongly affected by solar radiation such that they may experience substantial acceleration as well as exospheric losses due to photo-ionization. The recent observation of the extended Na tail on Mercury's night-side is strong evidence for radiation-pressure acceleration (Potter et al., 2002).

We can calculate the elevation angle $\alpha_j$ from particle velocity $\mathbf{v}_j$ and the vertical velocity component $v_{zj}$ (with $j = 0, 1, 2, 3, 4, 5, \ldots, n$, and $n$ the total number of altitude steps considered in the simulation):

$$\alpha_j = \arcsin\left(\frac{v_{zj}}{v_j}\right), \tag{9}$$

where $v_{zj}$ is the velocity component in $z$-direction, pointing away from the planetary surface and $\alpha_0$ is the ejection angle. Since we know the altitude step $\Delta z$ we can calculate the flight time $t_j$ for a particle for this step as

$$t_j = \frac{v_j \sin(\alpha_j)}{g(r)} - \left\{\left[\frac{v_j \sin(\alpha_j)}{g(r)}\right]^2 - \left(\frac{2\Delta z}{g(r)}\right)\right\}^{1/2}, \tag{10}$$

where $g$ is Mercury's gravitational acceleration as function of planetocentric distance $r$, $t_j$ is the flight time of each particle per altitude step. After knowing the flight time for an altitude step one can calculate the new $v_{z,j+1}$, $\mathbf{v}_{j+1}$ and $\alpha_{j+1}$ corresponding to the new altitude $z_{j+1}$ above the surface.

Figure 1 shows a few calculated ballistic trajectories for the thermal release of hydrogen, helium, sodium, and for sputtered calcium. Shown are the ejection angles of particles (elevation angle, Eq. (9)) along their trajectory from Mercury's surface to maximum height. The color coding of the points indicates the particle's energy at a particular height. In our study we follow each trajectory of the released particles by numerical integration until the particle hits the planetary surface again or leaves the calculation domain. Figure 1 covers the altitude range of the MPO spacecraft, with the horizontal line at 400 km height indicating the periherm distance. One can easily see that the scale height is strongly mass dependent. Thermally released hydrogen easily reaches the spacecraft altitudes, helium less, and sodium atoms rarely will reach even periherm altitudes. The sputtering process imparts more energy on the released particles, typical energies are a few eV. Thus, sputtered particles

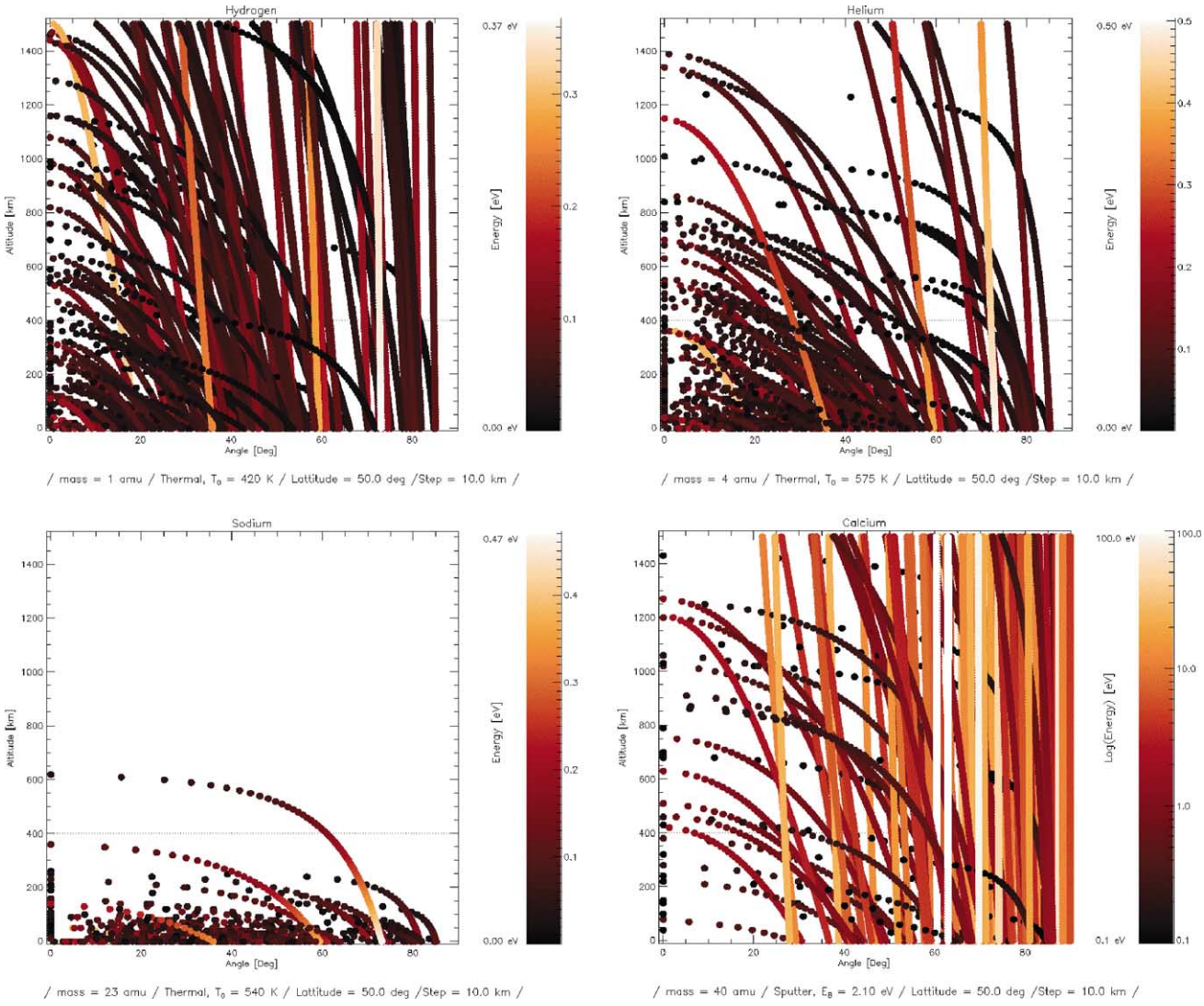


Fig. 1. Trajectories for the first hundred particles of a simulation for thermal release of hydrogen (upper left panel), helium (upper right panel), sodium (lower left panel), and for sputtered calcium atoms (lower right panel) for the altitude range of the MPO spacecraft. The angle is measured with respect to the surface plane (elevation angle); the color-coding gives the kinetic energy of the particles.

reach altitudes by far exceeding the MPO spacecraft altitude, which can be seen in the simulation for sputtered calcium.

## 4. Model generated density profiles of Mercury's exosphere

Using many calculated trajectories we can calculate the density profile of all different species if we know the release process and the associated parameters. The height dependent density is derived from

$$n(r) = n(z_i) = \tilde{n}\left(\frac{R_M}{r}\right)^2 \sum_j t_j, \tag{11}$$

where the sum extend over all particles $j$ that cross the surface located at height $r = R_M + i\,\Delta z$. At present we calculate height profiles but not the absolute densities and we scale the result to the measured or inferred exospheric data. The scaling factor $\tilde{n}$ is established either by prescribing a column density or a surface density that Eq. (11) has to reproduce. This procedure has been chosen because only composition data of the exosphere is available, but there are no data on the surface composition available.

In order to check our code we compare our results with measured data. Measured height profiles are available only for selected elements. For hydrogen and helium there are Mariner 10 data sets available (Hunten et al., 1988), and for calcium there are ground-based observations available (Bida et al., 2000). For hydrogen and helium we took the reported particle densities at the surface, for calcium we took the reported column density. A comparison between the calculated density profiles and the measured particle distribution is given in Fig. 2 for H, He, and Ca. For the thermal emission process, e.g., for H and He, the agreement be-

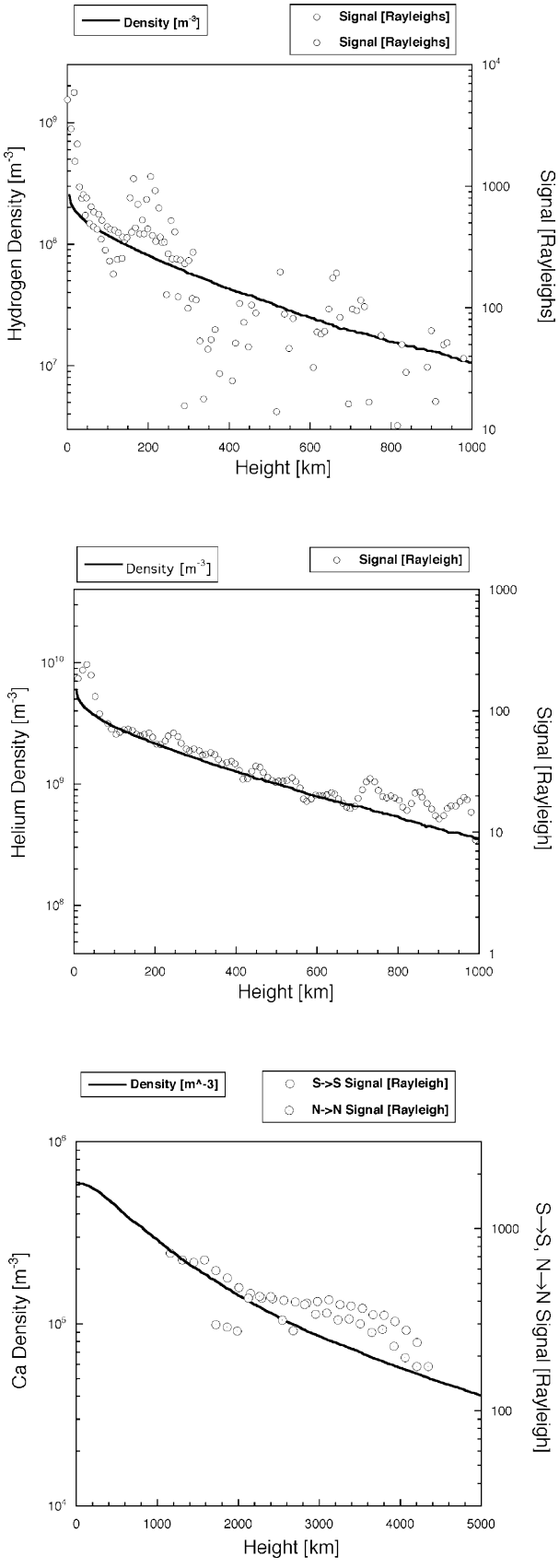


Fig. 2. Comparison of calculated densities for hydrogen (top panel), helium (middle panel), and calcium (bottom panel) and measured densities. See text for details.

tween measured and calculated data is satisfactory. Note that the calculation for hydrogen includes a cold component of $T_0 = 100$ K with a surface density of $23 \times 10^7$ m$^{-3}$ and a hot component of $T_0 = 420$ K with a surface density of $23 \times 10^6$ m$^{-3}$ (Hunten et al., 1988). The sum curve of these two components is given in Fig. 2 together with two data sets from Mariner 10 observations. For He only one component of $T_0 = 575$ K with a surface density of $6.0 \times 10^9$ m$^{-3}$ is necessary to reproduce the experimental data (Hunten et al., 1988). Ca is presumably sputtered from Mercury's surface because of the large optical line-width, which is interpreted as $T_0 = 12{,}000$ K, and the proximity of the Ca exospheric particles close to the poles of the planet where solar wind penetration may occur (Bida et al., 2000). Of course, the large temperature has to be interpreted as mean energy of 1.03 eV of the Ca atoms, which gives a binding energy of $E_\mathrm{b} = 2.1$ eV in Eq. (8). The result of our calculation for Ca together with two sets of Ca optical measurements from Bida et al. (2000) are given in Fig. 2. The agreement is not as good as for H and He, but still reasonable. Because of the high mean energies Ca has a large scale height in the exosphere. Since Ca is sputtered from the surface by solar wind there will be strong temporal as well as spatial variation of the Ca emission into the exosphere, which affects the measured data. Bida et al. (2000) already reported on the "apparently very dynamic Ca corona."

Note that our data in Fig. 2 are not fit to the experimental data, but arise from the calculation of the profile using the prescribed temperature or surface binding energy. Only the measured surface density or the column density are used as scaling parameter. It would be desirable to have more experimental data to check our code against. However, the lack of these data was exactly the reason why we developed the present code. In the future we will fully integrate the release processes into the code. Instead of calibrating to a surface density (or column density) we will start with a surface composition, calculate the released particle fluxes (due to solar UV photons, solar wind, micrometeorids, . . .), and finally the exospheric densities as we discussed above in the Sections 2.2 through 2.4 (Lammer et al., 2002). In order to be quantitative we need to know the exact surface composition, which is not known at present.

## 5. Results

We calculated density profiles for all elements and compounds reported in (Killen and Ip, 1999; Bida et al., 2000) since we wanted to study the possible mass spectrometric analysis of Mercury's exosphere (Mildner et al., 2001). We investigated all four release processes, thermal release, photon-stimulated desorption, micrometeorite impact vaporization and sputtering of particles, which were chosen depending of species to be released into the exosphere. The parameters for which the calculations were performed are listed in Table 1. Scaling the results from our Monte-Carlo

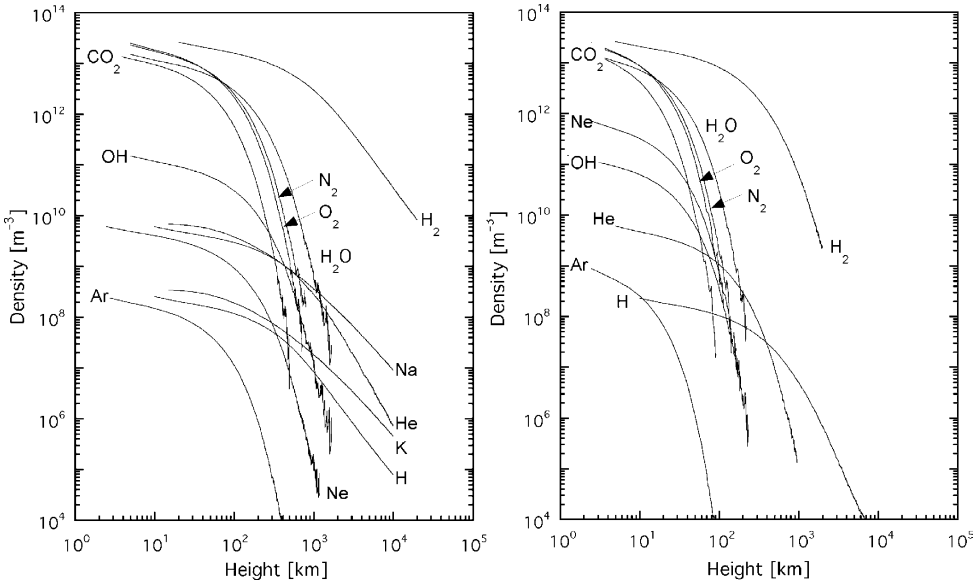


Fig. 3. Calculated exospheric densities for thermal emission for indicated species and PSD for Na and K at the day-side (left panel), at the night-side (right panel). See text for details.

calculation to absolute densities was done using either the surface density of the column density. Both approaches give the same density profile, however using the surface density relaxes the need to perform the calculations to large altitudes.

For modelling thermal release we used the local surface temperature given by Eq. (7). For PSD of Na and K we used the energy distribution given by Eq. (1) using a characteristic energy derived from the modified surface temperature $T_0$, as described in Section 2.1. Figure 3 shows the density profiles we obtained for the extremal cases, the day-side at a surface temperature of $T_0 = 540$ K and the night-side at $T_0 = 110$ K.

For modelling of micrometeorite impact vaporization we use thermal release with a characteristic temperature of $T_0 = 4000$ K. To obtain absolute densities we take the exospheric surface densities or column densities given in Table 1 divided by a factor of 100 based on the estimate given in Section 2.4.

Release by energetic ion sputtering is described by Eq. (8) using a characteristic energy $E_b$, the surface binding energy. Assessing the characteristic energy for the sputtering process is difficult since that parameter depends on the chemical environment of the element under consideration. Although the elemental, chemical and mineralogical composition of Mercury's surface is not well known, many elements are likely bound to oxygen. For example Na could be contained in feldspar ($NaAl_2Si_3O_8$). For physical sputtering of Na from a solid, i.e., the supra-thermal Na component, using a binding energy of $E_b \approx 2$ eV would be in agreement with laboratory measurements (Hofer, 1991). The measurement of the supra-thermal Na by Potter and Morgan (1997a) gave a density profile that was best fit by a barometric model with a temperature of $T_0 = 6500$ K, which relates to a binding energy of $E_b = 1.2$ eV. For the other sputtered elements we assume somewhat larger binding energies, which are given in Table 1. Since oxygen atoms are bound to the parent molecule/mineral even more tightly, the overall binding energy is expected to be in the range of 3–4 eV and we take 3.4 eV in our calculations. Using the energy distribution of Eq. (8), Na and O atoms are ejected with typical energies of about 1 and 1.7 eV. These energies compare well with observations and other estimates (Ip, 1986; Potter and Morgan, 1997a; Lammer and Bauer, 1997; Bida et al., 2000). Figure 4 shows the results of our calculation for micrometeorite impact vaporization and for particle sputtering. Micrometeorite impact vaporization will be homogenous over the whole planet, particle sputtering, on the contrary, will be very localized at places where (and when) the solar wind can reach the planet's surface.

## 6. Discussion

Thermal release of particles into the exosphere imparts only modest energy to the particles and the achieved altitudes of these particles are therefore limited, as can be seen from the results presented in Fig. 3. Even on the day-side the particle densities are low at the MPO spacecraft altitude (400 km at pericenter, 1500 km at apocenter). With a detection limit of $\approx 10^7$ m$^{-3}$ for the MAIA instrument on the MPO spacecraft, one can detect at pericenter all thermally released species but Ar listed in Table 1. Note that MAIA measures the particle flux rammed into its instrument entrance as a result of the spacecraft motion rather than measuring the local particle density. At apocenter only $H_2$, He, and $H_2O$ released thermally and Na and K released via PSD can be detected. The density fall-off within spacecraft altitude range is large. This in turn will allow the estimation of

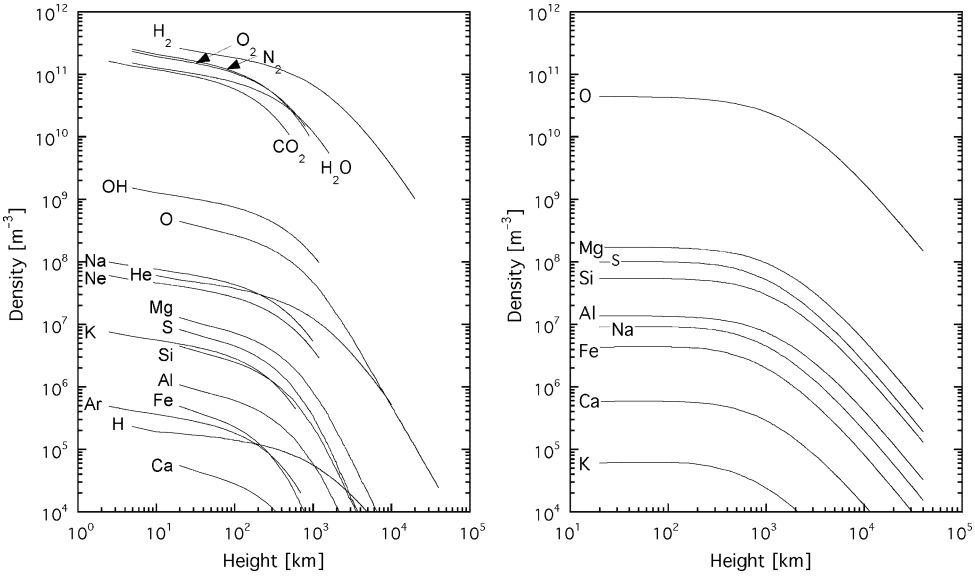


Fig. 4. Calculated exospheric densities for micrometeoritic impact vaporization (left panel), and sputtering (right panel). See text for details.

the characteristic temperature (or characteristic energy) of the emission process quite well from the density profile and finally one can derive the column densities of the species. On the night-side only H, $H_2$, and He can be detected at pericenter and only $H_2$ at apocenter. We have not considered release via PSD of Na and K on the night-side since it will not be operative there. However, Na and K will be accelerated toward the night-side by photon pressure (Ip, 1986, 1990). This has been observed recently with densities in the tail region being orders of magnitude lower than at the day-side of the planet (Potter et al., 2002).

Particle sputtering and micrometeorite impact impart more energy on the released particles and the resulting scale heights compare more favorably to the MPO spacecraft altitude. From the sputtered particles O, Mg, S, Si and Al are within the detection range (at least at pericenter) of MAIA and sputtered, e.g., supra-thermal, Na is marginally above the detection limit. Although the column densities for the refractory elements are considered to be quite high, the local particle densities in the exosphere are low since these particles are distributed over a large altitude range because of the large scale height resulting from the high energies from the sputter process. Since the scale height of sputtered elements is of the order of the MPO spacecraft altitude and higher, there is not a large change in densities over the spacecraft altitudes and therefore it will be more difficult to derive the characteristic energy and the column density than for thermally released particles.

From the measurement by the radio occultation experiment on Mariner 10 an upper limit of the ionospheric electron density was derived, and an upper limit of the atmospheric density of $10^{12}$ m$^{-3}$ was deduced from this measurement, corresponding to an exospheric pressure of $\approx 10^{-10}$ mbar (Fjelbo et al., 1976). Summing up our calculated exospheric surface densities of the known elements (H, He, O, Na, K, Ca) on the day-side results in a total exospheric gas density of $5 \times 10^{10}$ m$^{-3}$, which is almost two orders of magnitude less than the reported upper limit by Fjelbo et al. (1976). Considering all surface densities on the day-side results in a total exospheric gas density of $1.05 \times 10^{14}$ m$^{-3}$, which is two orders of magnitude higher than the reported upper limit. The exospheric density at the surface is dominated by volatile species that have not been measured so far and for those only an upper limit was given in the literature (Killen and Ip, 1999). So it may well be that these upper limits are considerably above the actual densities of these species. On the other hand, the deduction of the total surface density was questioned and it was argued the higher value from the EUV measurement of $10^{-9}$ mbar should be taken (Broadfoot et al., 1974; Hunten et al., 1988). Assuming a thermal gas at about 600 K results in an exospheric surface density of $10^{13}$ m$^{-3}$, still lower than the total density resulting from our calculation. Probably the densities of the volatile species reported in Table 1, $H_2$, $N_2$, $O_2$, $H_2O$, and $CO_2$, have to be reduced by at least an order of magnitude. However, a direct measurement will be necessary to decide on this issue.

## 7. Conclusions

In this paper we presented first results from a new Monte-Carlo code we developed in support of investigations of Mercury's exosphere by instrumentation intended for future Mercury missions. For the few experimental data sets available on Mercury's exosphere we find that our code reproduces these data reasonably well. For many other species we used reported column densities and the assumed release processes to model density profiles. Although there is quite some uncertainty in the various contributions to Mercury's

exosphere we can conclude that even an in situ measurement of local particle densities by mass spectrometric means seems feasible.

Based on our trajectory calculations we conclude that Mercury's exosphere will not reproduce small-scale features of the surface. Since particle emissions extend over large angular ranges and the characteristic energies are small substantial smearing of compositional surface features at spacecraft altitudes will occur even for sputtered particles. Therefore, the spatial resolution of an instrument measuring exospheric densities will be similar to the spacecraft altitude. Any fast changes in exospheric density, which may be observed from an orbiting spacecraft along its trajectory, will be due to temporal changes of the release of particles from the surface in agreement with earlier conclusions by Potter et al. (1999).

## References


Bida, T.A., Killen, R.M., Morgan, T.H., 2000. Discovery of calcium in Mercury's atmosphere. Nature 404, 159–161.

Broadfoot, A.L., Kumar, S., Belton, M.J.S., 1974. Mercury's atmosphere from Mariner 10: preliminary results. Science 185, 166–169.

Broadfoot, A.L., Shemansky, D.E., Kumar, S., 1976. Mariner 10: Mercury atmosphere. Geophys. Res. Lett. 3, 577–580.

Chase, S.C. Jr., Miner, E.D., Morrison, D., Münch, G., Neugebauer, G., 1976. Mariner 10 infrared radiometer results: temperatures and thermal properties of the surface of Mercury. Icarus 28, 565–578.

Cheng, A.F., Johnson, R.E., Krimigis, S.M., Lanzerotti, L.J., 1987. Magnetosphere, exosphere and surface of Mercury. Icarus 7, 430–440.

Cintala, M.J., 1992. Impact induced thermal effects in the lunar and mercurian regoliths. J. Geophys. Res. 97, 947–973.

Collier, M.R., Moore, T.E., Ogilvie, K.W., Chornay, D.J., Keller, J.W., Boardsen, S., Burch, J.L., El Marji, B., Fok, M.-C., Fuselier, S.A., Ghielmetti, A.G., Giles, B.L., Hamilton, D.C., Peko, B.L., Quinn, J.M., Stephen, T.M., Wilson, G.R., Wurz, P., 2001. Observations of neutral atoms from the solar wind. J. Geophys. Res. 106, 24893–24906.

Cooper, B., Potter, A., Killen, R., Morgan, T., 2001. Midinfrared spectra of Mercury. J. Geophys. Res. 106, 32803–32814.

Divine, N., 1993. Five populations of interplanetary meteoroids. J. Geophys. Res. 98, 17029–17048.

Eichhorn, G., 1978a. Heating and vaporization during hypervelocity particle impact. Planet. Space Sci. 26, 463–467.

Eichhorn, G., 1978b. Primary velocity dependence of impact ejecta parameters. Planet. Space Sci. 26, 469–471.

Fink, U., Larson, H.P., Popper, R.F., 1974. A new upper limit for an atmosphere of $CO_2$, CO on Mercury. Astrophys. J. 187, 407–415.

Fjelbo, G., Kliore, A., Sweetnam, D., Esposito, P., Seidel, B., Howard, T., 1976. The occultation of Mariner 10 by Mercury. Icarus 29, 407–415.

Goldstein, B.E., Suess, S.T., Walker, R.J., 1981. Mercury—magnetospheric processes and the atmospheric supply and loss rates. J. Geophys. Res. 86, 5485–5499.

Harmon, J.K., Slade, M.A., 1992. Radar mapping of Mercury—full disc images and polar anomalies. Science 258, 641–643.

Harmon, J.K., Perillat, P.J., Slade, M.A., 2001. High-resolution radar imaging of Mercury's north pole. Icarus 149, 1–15.

Heiken, G.H., Vaniman, D.T., French, B.M., 1991. Lunar Sourcebook. Cambridge Univ. Press, New York.

Hinton, F.L., Taeusch, D.R., 1964. Variation of the lunar atmosphere with the strength of the solar wind. J. Geophys. Res. 69, 1341–1347.

Hodges, R.R. Jr., 1973. Helium and hydrogen in the lunar atmosphere. J. Geophys. Res. 78, 8055–8064.

Hodges, R.R. Jr., 1980. Methods for Monte-Carlo simulation of the exospheres of the Moon and Mercury. J. Geophys. Res. 85, 164–170.

Hofer, W.O., 1991. Angular, energy, and mass distribution of sputtered particles. In: Behrisch, R., Wittmaack, K. (Eds.), Sputtering by Particle Bombardment, pp. 15–90.

Hunten, D.M., Morgan, T.M., Shemansky, D.E., 1988. The Mercury atmosphere. In: Vilas, F., Chapman, C.R., Matthews, M.S. (Eds.), Mercury. University of Arizona Press, Tucson, pp. 562–613.

Ip, W.-H., 1986. The sodium exosphere and magnetosphere of Mercury. Geophys. Res. Lett. 13, 423–426.

Ip, W.-H., 1990. On solar radiation-driven surface transport of sodium atoms at Mercury. Astrophys. J. 356, 675–681.

Johnson, F.S., 1971. Lunar atmosphere. Rev. Geophys. Space Phys. 9, 813–823.

Johnson, R.E., 1990. Energetic Charged Particle Interactions with Atmospheres and Surfaces. Springer-Verlag, Berlin/Heidelberg/New York.

Johnson, R.E., Leblanc, F., Yakshinskiy, B.V., Madey, T.E., 2002. Energy distributions for desorption of sodium and potassium from ice: the Na/K ratio at Europa. Icarus 156, 136–142.

Jursa, A.S. (Ed.), 1985. Handbook of Geophysics and the Space Environment. Air Force Geophysical Laboratory.

Kabin, K., Gombosi, T.I., DeZeeuw, D.L., Powell, K.G., 2000. Interaction of Mercury with the solar wind. Icarus 143, 397–406.

Killen, R.M., Potter, A.E., Morgan, T.H., 1990. Spatial distribution of sodium vapor in the atmosphere of Mercury. Icarus 85, 145–167.

Killen, R.M., Morgan, T.H., 1993. Maintaining the Na atmosphere of Mercury. Icarus 101, 294–312.

Killen, R.M., Ip, W.-H., 1999. The surface-bounded atmospheres of Mercury and the Moon. Rev. Geophys. 37, 361–406.

Killen, R.M., Potter, A., Fitzsimmons, A., Morgan, T.H., 1999. Sodium D2 line profiles: clues to the temperature structure of Mercury's exosphere. Planet. Space Sci. 47, 1449–1458.

Killen, R.M., Potter, A.E., Reiff, P., Sarantos, M., Jackson, B.V., Hick, P., Giles, B., 2001. Evidence for space weather at Mercury. J. Geophys. Res. 106, 20509–20525.

Kumar, S., 1976. Mercury's atmosphere: a perspective after Mariner 10. Icarus 28, 579–591.

Lammer, H., Bauer, S.J., 1997. Mercury's exosphere: origin of surface sputtering and implications. Planet. Space Sci. 45, 73–79.

Lammer, H., Kolb, C., 2001. Release processes of exospheric particles from Mercury's surface. Internal IWF Report. Space Research Institute Austrian Academy of Sciences, No. 136, pp. 1–23.

Lammer, H., Wurz, P., Patel, M.R., Killen, R., Kolb, C., Massetti, S., Orsini, S., Milillo, A., 2002. The variability of Mercury's exosphere by particle and radiation induced surface release processes. Icarus. Submitted.

Langevin, Y., 1997. The regolith of Mercury: present knowledge and implications for the Mercury Orbiter mission. Planet. Space Sci. 45, 31–37.

Luhmann, J.G., Russell, C.T., Tsyganenko, N.A., 1998. Disturbances in Mercury's magnetosphere: are the Mariner 10 "substorms" simply driven? J. Geophys. Res. 103, 9113–9119.

Massetti, S., Orsini, S., Milillo, A., Mura, A., De Angelis, E., Lammer, H., Wurz, P., 2002. Mapping of the cusp plasma precipitation on the surface of Mercury. Icarus. Submitted.

McGrath, M.A., Johnson, R.E., Lanzerotti, L.J., 1986. Sputtering of sodium on the planet Mercury. Nature 323, 694–696.

Mildner, M., Wurz, P., Scherer, S., Zipperle, M., Altwegg, K., Bochsler, P., Benz, W., Balsiger, H., 2001. Measurement of neutral atoms and ions in Mercury's exosphere. Planet. Space Sci. 49 (1415), 1655–1658.

Morgan, T.H., Zook, H.A., Potter, A.E., 1988. Impact-driven supply of sodium to the atmosphere of Mercury. Icarus 75, 156–170.

Morgan, T.H., Zook, H.A., Potter, A.E., 1989. Production of sodium vapor from exposed regolith in the inner solar system. In: Proc. Lunar Planet. Sci. Conf. 19th, pp. 297–304.

Ness, N.F., Behannon, K.W., Lepping, R.P., Whang, Y.C., Schatten, K.H., 1974. Magnetic field observations near Mercury: preliminary results from Mariner 10. Science 185, 151–160.

Ness, N.F., Behannon, K.W., Lepping, R.P., Whang, Y.C., Schatten, K.H., 1976. Observations of Mercury's magnetic field. Icarus 28, 479–488.

Ogilvie, K.W., Scudder, J.D., Hartle, R.E., Siscoe, G.L., Bridge, H.S., Lazarus, A.J., Asbridge, J.R., Bame, S.J., Yeates, C.M., 1974. Observations at Mercury encounter by the plasma science experiment on Mariner 10. Science 185, 146–152.

Potter, A., Morgan, T.H., 1985. Discovery of sodium in the atmosphere of Mercury. Science 229, 651–653.

Potter, A., Morgan, T.H., 1986. Potassium in the atmosphere of Mercury. Icarus 67, 336–340.

Potter, A., Morgan, T.H., 1997a. Evidence of suprathermal sodium on Mercury. Adv. Space Res. 19 (19), 1571–1576.

Potter, A., Morgan, T.H., 1997b. Sodium and potassium atmospheres of Mercury. Planet. Space Sci. 45 (1), 95–100.

Potter, A., Killen, R.M., Morgan, T.H., 1999. Rapid changes in the sodium exosphere of Mercury. Planet. Space Sci. 47, 1441–1448.

Potter, A., Killen, R.M., Morgan, T.H., 2002. The sodium tail of Mercury. Meteor. Planet. Sci. 37 (9), 1165–1172.

Russell, C.T., Baker, D.N., Slavin, J.A., 1988. The magnetosphere of Mercury. In: Vilas, F., Chapman, C.R., Matthews, M.S. (Eds.), Mercury. The University of Arizona Press, Tucson, pp. 514–561.

Sarantos, M., Reiff, P.H., Hill, T.W., Killen, R.M., Urquhart, A.L., 2001. A $B_x$-interconnected magnetosphere model for Mercury. Planet. Space Sci. 49, 1629–1635.

Sieveka, E.M., Johnson, R.E., 1984. Ejection of atoms and molecules from Io by plasma-ion impact. Astrophys. J. 287, 418–426.

Sigmund, P., 1969. Theory of sputtering. I. Sputtering yield of amorphous and polycrystalline targets. Phys. Rev. 184, 383–416.

Smyth, W.H., Johnson, R.E., 1984. Nature and variability of Mercury's sodium atmosphere. Nature 323, 696–699.

Sprague, A.L., 1990. A diffusion source for sodium and potassium in the atmospheres of Mercury and the Moon. Icarus 84, 93–105.

Sprague, A.L., Hunten, D., Lodders, K., 1995. Sulfur at Mercury, elemental at the poles and sulfides in the regolith. Icarus 118, 211–215.

Sprague, A.L., Kozlowski, R.W.H., Hunten, D.M., Schneider, N.M., Domingue, D.L., Kells, W.K., Schmitt, W., Fink, U., 1997. Distribution and abundance of sodium in Mercury's atmosphere, 1985–1988. Icarus 129, 506–527.

Sprague, A.L., Schmitt, W.J., Hill, R.E., 1998. Mercury: sodium atmospheric enhancements, radar-bright spots, and visible surface features. Icarus 136, 60–68.

Starukhina, L.V., 2000. High radar response of Mercury polar regions: water ice or cold silicates? Lunar. Planet. Sci. XXXII, 1301. (Abstract).

Wurz, P., Blomberg, L., 2001. Particle Populations in Mercury's Magnetosphere. Planet. Space Sci. 49 (1415), 1643–1653.

Yakshinskiy, B.V., Madey, T.E., 1999. Photon-stimulated desorption as a substantial source of sodium in the lunar atmosphere. Nature 400, 642–644.

Yakshinskiy, B.V., Madey, T.E., 2001a. Electron- and photon-stimulated desorption of K from ice surfaces. J. Geophys. Res. 106, 33303–33308.

Yakshinskiy, B.V., Madey, T.E., 2001b. Electron- and photon-stimulated desorption of alkali atoms (Na, K) from water ice and silicon surfaces. Lunar. Planet. Sci. XXXII, 1896. (Abstract).

Zelen, M., Severo, N.C., 1965. Probability functions. In: Abramowitz, M., Stegun, A. (Eds.), Handbook of Mathematical Functions. Dover, New York.